Applied Surface Science 497 (2019) 143771

Contents lists available at ScienceDirect

Applied Surface Science

journal homepage: www.elsevier.com/locate/apsusc

Full length article

An urchin-like Ag_3PO_4/Pd/$LaPO_4$ photocatalyst with *Z*-scheme heterojunction for enhanced hydrogen evolution

Xi Chen[a,b], Wenwen Zhang[b], Lixiang Zhang[c,b], Luping Feng[a,b], Jiangwei Wen[b], Jianjing Yang[b], Chunxian Zhang[b], Jie Jiang[d], Hua Wang[a,b,d,*]

[a] School of Chemistry and Chemical Engineering, Harbin Institute of Technology, Harbin, Heilongjiang 150090, PR China
[b] Institute of Medicine and Materials Applied Technologies, College of Chemistry and Chemical Engineering, Qufu Normal University, Qufu, Shandong 273165, PR China
[c] School of Environment, Harbin Institute of Technology, Harbin, Heilongjiang 150090, PR China
[d] School of Marine Science and Technology, Harbin Institute of Technology at Weihai, Weihai, Shandong 264209, PR China

ARTICLE INFO

Keywords:
Ag_3PO_4/Pd/$LaPO_4$
Urchin-like morphology
Self-assembly
Synergistic photocatalysis
Z-scheme system

ABSTRACT

An urchin-like $LaPO_4$-based nanocomposite integrating Ag_3PO_4 and Pd has been initially synthesized via a controllable self-assembly route, with enhanced photocatalysis and ultrastable structure for the synergistic hydrogen (H_2) evolution under sunlight. Citric acid was employed as a structure-mediated agent to guide the oriented growth of $LaPO_4$ along [101] facet at room temperature, showing the urchin-like 3D structure. Furthermore, Pd and Ag_3PO_4 were coated in turn resulting in the Ag_3PO_4/Pd/$LaPO_4$ nanocomposite, in which Pd and Ag_3PO_4 could act as the functions of electron receptor and electron donor in the photocatalysis, respectively. It was discovered that the as-developed nanocomposite could present the robust photocatalysis and stable morphology after consecutive uses. Based on the band structure analysis, a *Z*-scheme system of Ag_3PO_4/Pd/$LaPO_4$ was thereby proposed for the sunlight photocatalysis, as testified by DMPO spin trapping ESR spectra. Also, the photoluminescence and electrochemical impedance of nanocomposites were conducted, indicating that the improved carriers properties should be responsible mainly for the dramatically enhanced photocatalytic activities. Moreover, the outstanding photocatalytic performances of Ag_3PO_4/Pd/$LaPO_4$ were demonstrated in H_2 evolution (1084.3 $\mu mol \cdot g^{-1} \cdot h^{-1}$) under sunlight. Importantly, such a citric acid-controlled self-assembly route may pave the way toward the fabrication of multi-component photocatalyst tailored for the wide photocatalytic applications.

1. Introduction

Up to date, semiconductor photocatalysts have been extensively fabricated for many photocatalytic applications like hydrogen generation of water splitting and removals of organic pollutants [1,2]. Moreover, in order to achieve more efficient photocatalysis performances especially under sunlight, the synthesis of various photocatalytic composites by integrating functional materials has been preferably explored in recent years [3–7]. For example, You et al. demonstrated g-C_3N_4 nanorods integrated with hollow $InVO_4$ nanospheres could allow for the enhanced photocatalytic degradation of methylene blue [8]. Lu and coworks reported that Ni_2P dispersed with g-C_3N_4 could realize the highly efficient photocatalytic H_2 evolution [9]. Nevertheless, most of the current photocatalysts composed of functional elements can be trapped by some formidable disadvantages such as the complicated preparation, structural instability, and especially low synergistic photocatalysis efficiency, which may have challenged their practical applications on a large scale.

Recent years has witnessed the rapid development of metal phosphates as promising photocatalytic nanomaterials [10,11]. As a particular member of such family, $LaPO_4$ has attracted increasing attentions for the photocatalytic applications [12,13]. It is widely recognized that $LaPO_4$ can display a preeminent capacity for electron reduction due to its more negative conduction band potential, of which the photogenerated electrons with strong reduction can readily restore H_2O into H_2. Yet, some inhere defects of $LaPO_4$ have enormously limited its practical photocatalytic applications, such as functional singleness, low conductivity, and especially high recombination of photo-induced electron-holes leading to low photocatalysis. Hence, it is of great interest to integrate some functional elements to synergistically enhance the photocatalysis performances of the $LaPO_4$-based photocatalysts. Moreover, as another important member of metal phosphates, Ag_3PO_4

* Corresponding author at: School of Chemistry and Chemical Engineering, Harbin Institute of Technology, Harbin, Heilongjiang, 150090, PR China.
E-mail address: huawang@qfnu.edu.cn (H. Wang).

https://doi.org/10.1016/j.apsusc.2019.143771
Received 10 July 2019; Received in revised form 4 August 2019; Accepted 22 August 2019
Available online 23 August 2019
0169-4332/

has concentrated great efforts in the photocatalysis field because of its excellent quantum efficiency over visible light area [14–17]. Alternatively, Ag_3PO_4 has been employed as a photosensitizer or active site to be modified on other photocatalysts. For example, Liu's group found that Ag_3PO_4 nanoparticles in situ grown on the surface of two-dimensional $MoSe_2$ nanoarchitectures could act as a noble metal-free cocatalyst for photocatalytic oxygen evolution under LED-light irradiation [18]. Yang et al. reported g-C_3N_4 nanorods integrated with Ag_3PO_4 using Ag and graphene as mediators showing the enhanced photocatalytic performances for water oxidation [19]. Besides, photocatalyst integrated with Ag_3PO_4 has been usually testified forming a *Z*-scheme heterojunction distinguished from the conventional heterojunction. Specifically, the reduced metallic Ag nanoparticles can play a role as the electron mediator in promoting the separation and transferring of charge carriers on Ag surfaces, resulting in the *Z*-scheme mechanism for improved photocatalysis [20,21].

In the present work, we seek to employ the self-assembly route to synthesize an urchin-like $LaPO_4$ nanorods by using citric acid as the structure-mediated agent, followed by the integration of functional materials of Pd and Ag_3PO_4. The resulting nanocomposites could display dramatically enhanced photocatalysis for the synergistic H_2 evolution, due to their improved carriers transferring and especially synergistic photocatalysis efficiency of self-assembled elements. Also, an extremely stable urchin-like structure, instead of a simple mixture, could be expected for the resulting nanocomposites, showing a preeminent specific surface area together with numerous unsaturated active sites exposed from their poignant profile. Also, photosensitive Ag_3PO_4 would be decomposed to produce Ag elements serving as the bridge for transferring photogenerated electrons so as to efficiently construct the *Z*-scheme heterojunction to endow the enhanced photocatalytic activity of Ag_3PO_4-Pd/$LaPO_4$, of which the efficient photocatalysis performances were subsequently demonstrated in photocatalytic H_2 evolution. The fabrication procedure and main photocatalytic mechanism of Ag_3PO_4/Pd/$LaPO_4$ nanocomposite is schematically illustrated in Scheme 1. To the best of our knowledge, this is the first report on the fabrication of an urchin-like photocatalyst of $LaPO_4$-based nanocomposite integrating functional elements of Pd and Ag_3PO_4 by the controllable self-assembly route, achieving the enhanced photocatalysis and ultrastable structure for synergistic H_2 evolution under sunlight.

2. Experimental section

2.1. Materials and instruments

$La(NO_3)_3{\cdot}6H_2O$ (99.0%) was purchased from Sigma-Aldrich Co. Ltd. (Shanghai, China). $Pd(C_2H_3O_2)_2$ (Pd ≥ 47.0%) was obtained from Dibai Biotechnology Co. Ltd. (Shanghai, China). $AgNO_3$ (99.8%), $Na_3PO_4{\cdot}12H_2O$ (98.0%) and $C_6H_8O_7{\cdot}H_2O$ (99.5%) were obtained from Sinopharm Chemical Reagent Co. Ltd. (Shanghai, China). H_3PO_4 (85.0%) was bought from Kaitong Chemical Co. Ltd. (Tianjin, China). Lactic acid, ethanol, and TiO_2 powders are commercially available of analytical grade and used as received. Deionized water (> 18.2 Megohm/cm), which was obtained from an ultra-pure water system (Pall, USA), was used for the preparation of all solutions. LabSolar-III AG photocatalytic on-line analysis system was bought from PerfectLight Technology Co. Ltd. (Beijing, China).

2.2. Preparation of photocatalytic materials

2.2.1. Synthesis of $LaPO_4$

Typically, 216.5 mg of lanthanum nitrate and 50 mg of citric acid were dissolved in 50 mL deionized water. An aliquot of 30 μL of phosphoric acid was added in 5 mL water and then slowly dropped into the above mixture to be stirred for 30 min at room temperature. The resulting $LaPO_4$ white precipitate was centrifuged and washed with water and ethanol each for several times. Finally, the obtained $LaPO_4$ products were calcined at 200 °C for 2 h and further collected in the dryer. In addition, the preparation of Ag_3PO_4 was detailed in supporting information.

2.2.2. Synthesis of Pd/$LaPO_4$

Typically, an aliquot of 150 mg of $LaPO_4$ powder and 1.6 mg of palladium acetate were dispersed in 30 mL ethanol. The mixture was

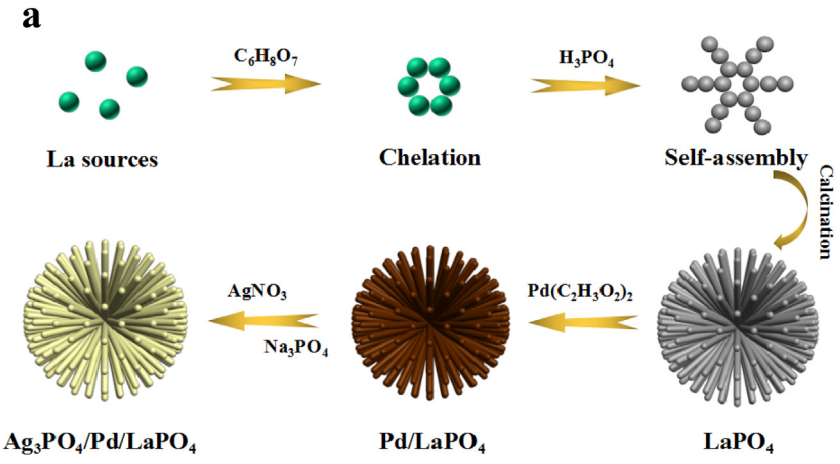

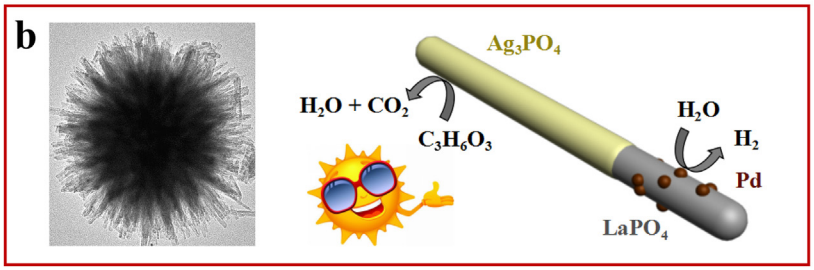

Scheme 1. (a) Schematic illustration of fabrication procedure and mechanism of the urchin-like Ag_3PO_4/Pd/$LaPO_4$ nanocomposite including citric acid-La^{3+} chelation, phosphoric acid-triggered $LaPO_4$ self-assembly, calcination toward $LaPO_4$, Pd coating on $LaPO_4$ toward Pd/$LaPO_4$, and Ag_3PO_4 in-situ growth on Pd/$LaPO_4$ yielding the Ag_3PO_4/Pd/$LaPO_4$. (b) The photocatalytic mechanism of Ag_3PO_4/Pd/$LaPO_4$ nanocomposite exemplified by using one nanorod with the Ag_3PO_4 coating partly peeled, showing the urchin-like structure typically in TEM image (left) for the H_2 evolution under sunlight.

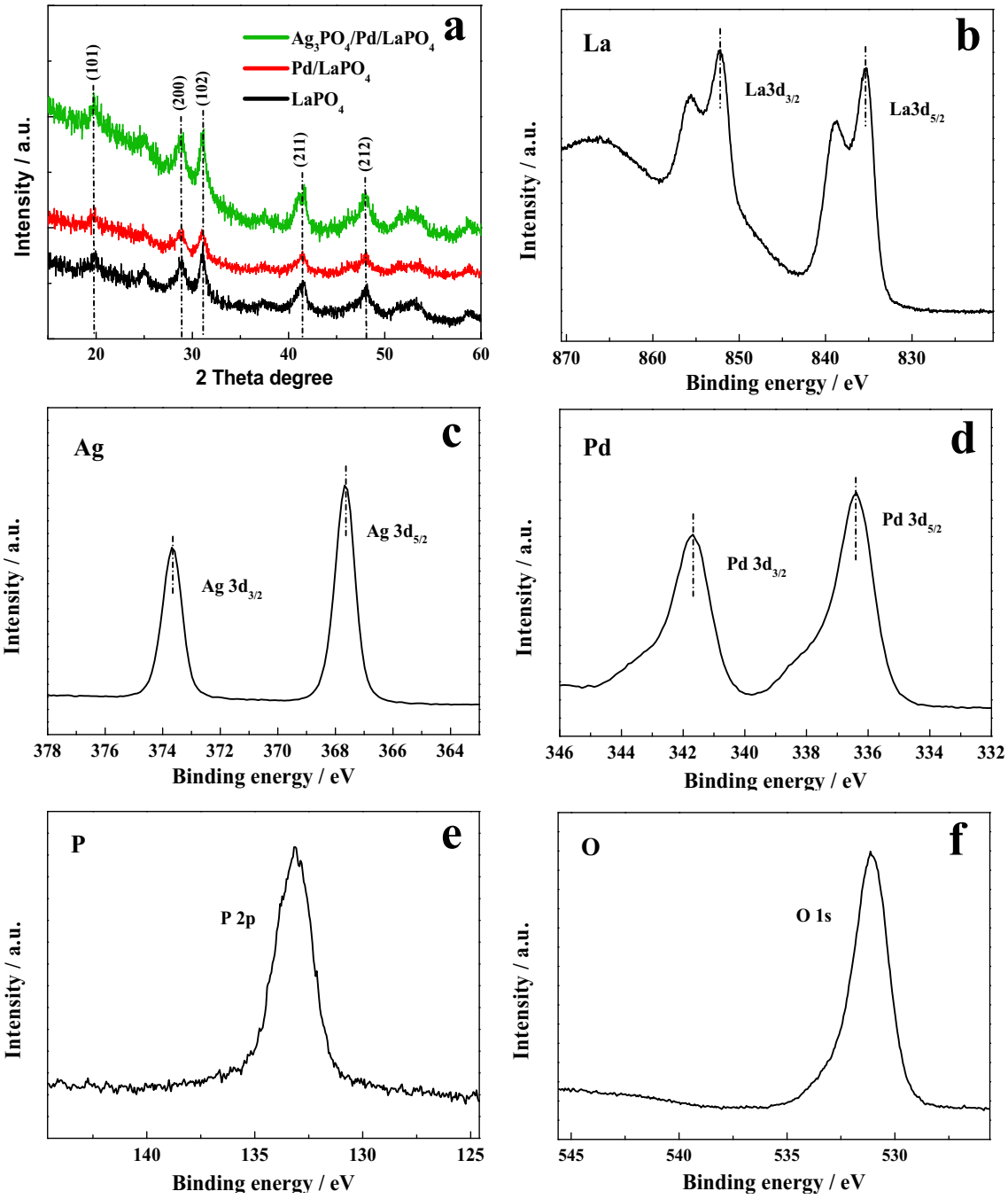

Fig. 1. (a) XRD patterns of different samples; XPS spectra of (b) La 3d, (c) Ag 3d, (d) Pd 3d, (e) P 2p, and (f) O 1s.

sonicated for 5 min, and then stirred in the dark overnight. The obtained gray product of $Pd/LaPO_4$ was washed with ethanol to eliminate the impurities, followed by being dried at 60 °C for 12 h.

2.2.3. Synthesis of $Ag_3PO_4/Pd/LaPO_4$

In a typical synthesis route, 200 mg of $Pd/LaPO_4$ powder was dispersed into 10 mL water, followed by adding 4.9 mg of silver nitrate. Furthermore, 3.6 mg of sodium phosphate was dissolved in 10 mL water and then added drop by drop into the above mixture to be stirred for 1 h in dark. The resultant $Ag_3PO_4/Pd/LaPO_4$ nanocomposites were centrifuged and washed with water and ethanol for several times, and subsequently dried at 60 °C to be further stored in the dryer.

2.3. Characterization of photocatalytic materials

The phase compositions of the prepared products were determined by X-ray diffraction (XRD, PANalytical/X'pert3). The diffraction patterns were recorded in the range of $2\theta = 15°–60°$ using Cu Kα radiation. X-ray photoelectron spectra (XPS) were determined by a spectrometer (ESCALAB 250Xi) using Al Kα radiation. The morphological structures of the materials were examined separately by the field emission scanning electron microscopy (SEM, JEOL/JSM-6700F and Carl Zeiss AG/Sigma 500 VP) with electron energy of 5 kV and the transmission electron microscopy (TEM, JEOL/JEM-2100PLUS). The inductively coupled plasma (ICP) tests were carried out by an emission spectrometer (ICP/2060 T). The optical properties of material samples, i.e., UV–vis diffuse reflection spectra (DRS), were explored by UV-3600

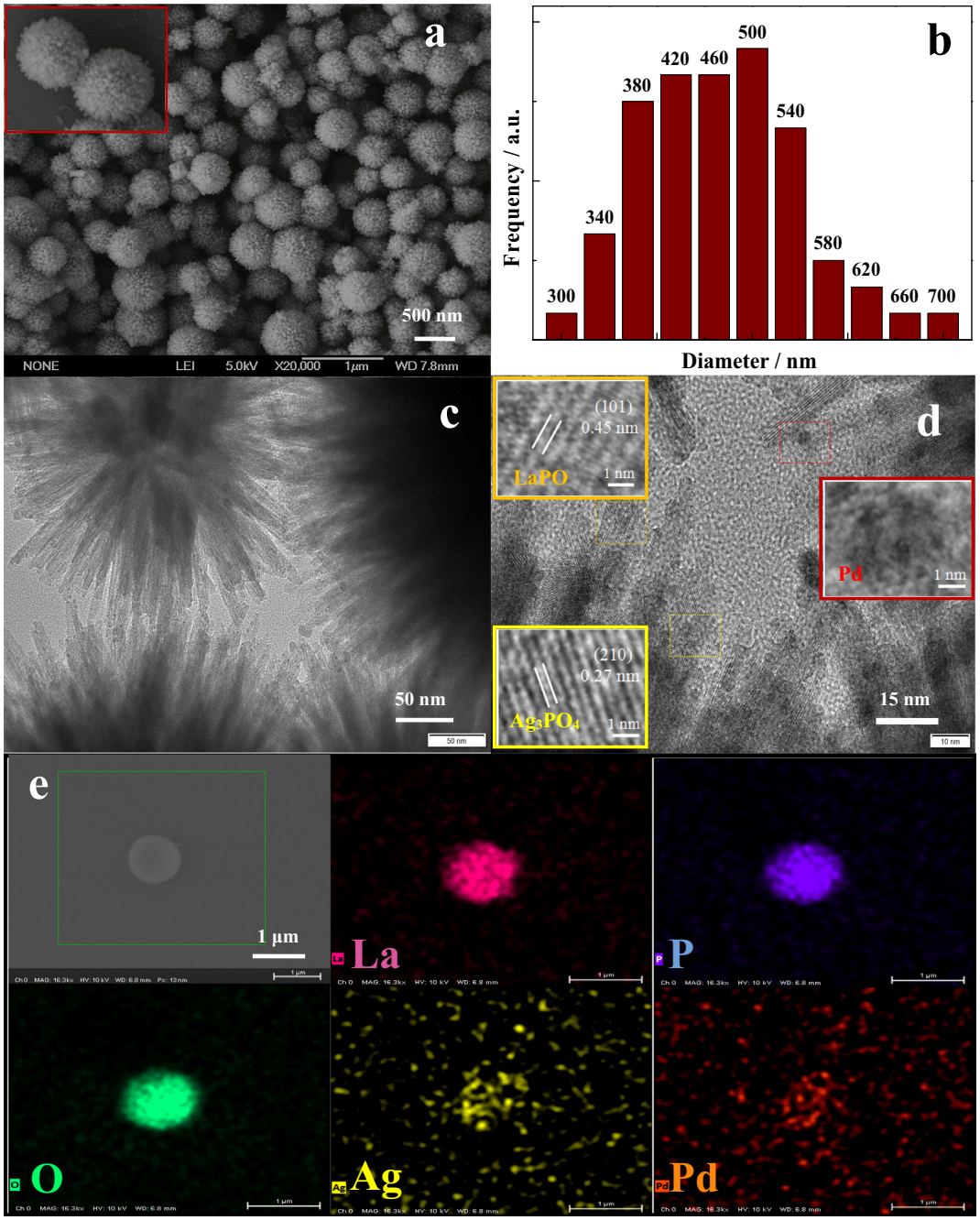

Fig. 2. (a) SEM images and (b) size distribution of Ag_3PO_4/Pd/$LaPO_4$ nanocomposites; (c–d) TEM images of Ag_3PO_4/Pd/$LaPO_4$ of different magnifications; (e) EDS element mapping of Ag_3PO_4/Pd/$LaPO_4$ composing of O, P, La, Ag, and Pd elements.

spectrophotometer (Shimadzu, Japan) using $BaSO_4$ as reference in the range of 250–700 nm. The photoluminescence spectra of the samples were measured using the fluorescence spectrometer (Horiba/FluoroMax-4). DMPO electron spin resonance (ESR) tests were conducted by a spectrometer (JEOL/JES-FA200) to prove the existence of $\cdot O_2^-$ and ·OH in the photocatalytic reactions. The electrochemical workstation (CHI 760D) was used to record the electrochemical impedance spectroscopy (EIS) using a platinum plate and a saturated calomel electrode as the counter electrode and reference electrode, respectively. The working electrode was made by dip-coating a sample slurry (5 mg·mL^{-1} in ethanol) on titanium plate with the area at 1.5 × 1.0 cm, followed by air drying, and 0.10 M KCl solution was used as the electrolyte.

2.4. Photocatalytic H_2 evolution experiments

The activities of photocatalytic materials in the photocatalytic H_2 evolution reactions were investigated under simulated sunlight irradiation by using LabSolar-III AG photocatalytic on-line analysis system similar to the previous report [22]. Typically, an aliquot of 0.1 g of photocatalysts was dispersed in 45 mL of water. Further, 5 mL of lactic acid was added as the sacrificial reagent for the holes capture. The simulated sunlight source of a 300 W Xe-lamp (PerfectLight Technology Co. Ltd., PLS-SXE300) was placed 20 cm apart from the reaction solution. The temperature of reaction solution was kept at 15 ± 2 °C by cooling water. At given time intervals, H_2 concentrations so evolved were determined online using the gas chromatography (Agilent Technologies Co. Ltd., GC-7890B, MS-5A column, TCD, N_2 carrier).

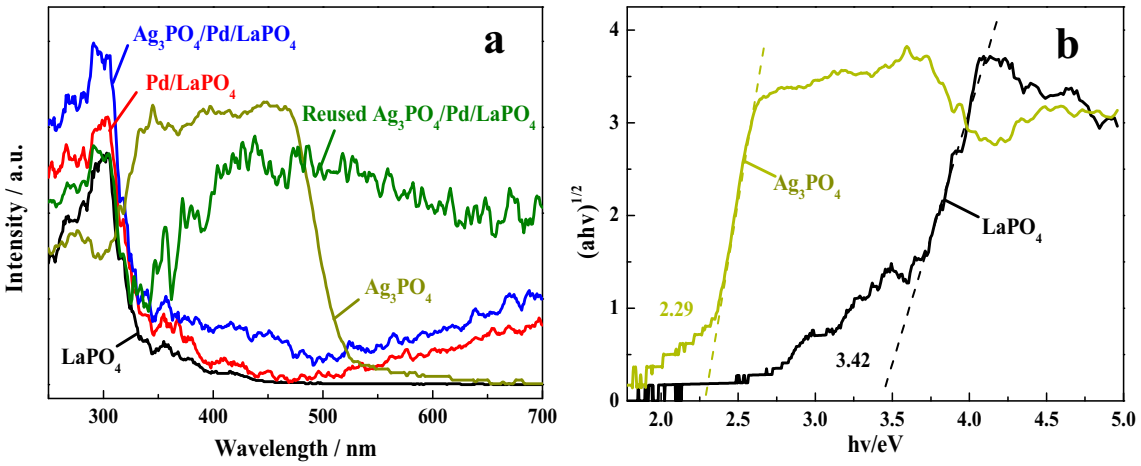

Fig. 3. (a) UV–vis/DRS spectra of different photocatalyst samples; (b) plots of $(ahv)^{1/2}$ versus hv of Ag_3PO_4 and $LaPO_4$.

3. Results and discussion

3.1. Fabrication and characterization of Ag_3PO_4/Pd/$LaPO_4$

The fabrication procedure of Ag_3PO_4/Pd/$LaPO_4$ nanocomposite is schematically illustrated in Scheme 1a. Herein, during the controlled self-assembly synthesis of urchin-like $LaPO_4$ photocatalyst, La^{3+} ions were coordinated with citric acid, and reunited together to form the La^{3+}-citric acid complex. When H_3PO_4 was subsequently added in above system, the crystals grew along the [101] direction to develop the urchin-like structure of $LaPO_4$, which was subsequently stabilized by calcination. Afterwards, Pd nanoparticles (high work function) were deposited, aiming to restrain the recombination of carriers to achieve more reduction sites of photogenerated electrons of $LaPO_4$, and significantly strengthened the visible light absorption [23,24]. The resulting Pd/$LaPO_4$ was further coated with Ag_3PO_4 to yield the Ag_3PO_4/Pd/$LaPO_4$ nanocomposites. Thereunto, Ag_3PO_4 would be decomposed to produce Ag elements (low work function) to serve as the bridges between $LaPO_4$ and Ag_3PO_4 for boosting the transferring of photogenerated electrons. [25,26]. The main photocatalytic mechanism of Ag_3PO_4/Pd/$LaPO_4$ nanocomposite was described in Scheme 1b, which would be discussed in more detail afterwards.

The crystal structure of the prepared Ag_3PO_4/Pd/$LaPO_4$ photocatalyst was determined by comparing to Pd/$LaPO_4$ and $LaPO_4$ using the X-ray powder diffraction (XRD) patterns (Fig. 1a). Accordingly, the Ag_3PO_4/Pd/$LaPO_4$ has the diffraction peaks at 19.8°, 28.9°, 31.2°, 41.5°, and 48.0° corresponding to the (101), (200), (102), (211) and (212) facets, respectively, indexed for the crystalline phase of hexagonal $LaPO_4$ (JCPD standard card No.46-1439) [27]. It was a pity that no significant diffraction peaks of Ag_3PO_4 or Pd were observed for the nanocomposite, which might presumably due to that Pd and Ag_3PO_4 were highly dispersed on the surface of the $LaPO_4$ with relatively low amounts [21,28].

The chemical states of contributed elements on the surface of Ag_3PO_4/Pd/$LaPO_4$ were investigated by X-ray photoelectron spectroscopy (XPS) with the results shown in Fig. 1b–f. The binding energies of 835.5 and 852.3 eV observed from Fig. 1b belong to the La^{3+} in nanocomposite [13]. Two individual peaks situated at 367.7 and 373.7 eV are associated to Ag3$d_{5/2}$ and Ag3$d_{3/2}$, proving that the chemical state of Ag is monovalent (Fig. 1c) [29]. The signals at 336.4 and 341.6 eV are assigned to Pd3$d_{5/2}$ and Pd3$d_{3/2}$ can be revealed that Pd is mainly in the state of Pd^0 (Fig. 1d) [30]. The characteristic signals of P2p (Fig. 1e) and O1s (Fig. 1f) are peaks of P^{5+} and O^{2-}, respectively [31]. Hence, the results further verify the successful fabrication of Ag_3PO_4/Pd/$LaPO_4$.

Moreover, the morphology features of Ag_3PO_4/Pd/$LaPO_4$ products were characterized separately using scanning electronic microscopy (SEM) and transmission electronic microscopy (TEM) (Fig. 2). It was found that $LaPO_4$ could present the urchin-like 3D structure composed of massive nanorods (Fig. S2). After the deposition of Pd and Ag_3PO_4 elements, the yielded Ag_3PO_4/Pd/$LaPO_4$ could evidently retain the orientation accumulation of nanorods (Fig. 2a), which could feature the high dispersity with the rod length of 190–270 nm (Fig. 2b). Importantly, the well retained urchin-like structure of Ag_3PO_4/Pd/$LaPO_4$ would provide a large surface area to enhance the contact of the photocatalysts with water and lactic acid afterwards, which would help to improve the photocatalytic activity in the H_2 evolution. Also, urchin-like Ag_3PO_4/Pd/$LaPO_4$ could be topologically composed of numerous nanorods, with the average size of about 10 nm in diameter (Fig. 2c), which could help to improve the separation of photogenerated carriers subsequently. Moreover, one can note from Fig. 2d that the lattices, which were measured from the selected areas, illustrate the spacings of 0.45 nm and 0.27 nm, corresponding to the (101) lattice facet of hexagonal $LaPO_4$ and the (210) lattice plane of cubic Ag_3PO_4, respectively. Pd nanoparticles deposited on nanocomposites can present an average size of about 5.0 nm in diameter. Moreover, high-resolution TEM imaging was further performed for Ag_3PO_4/Pd/$LaPO_4$ to explore the presence of Ag_3PO_4 with the results shown in Fig. S3, showing that Ag_3PO_4 nanoparticles (indicated with red arrows) were coated on $LaPO_4$ nanorods. In addition, X-ray energy dispersive spectroscopy (EDS) elemental mapping was employed to probe the spatial distribution of chemical elements of Ag_3PO_4/Pd/$LaPO_4$ with disparate color contrasts (Fig. 2e). As expected, the elements of O, P, La, Ag, and Pd could be uniformly distributed on the surface of the nanocomposites. Besides, the contents of Pd and Ag in Ag_3PO_4/Pd/$LaPO_4$ were determined by ICP measurements, with the data listed in Table S1.

The optical absorption properties of the prepared photocatalysts were further explored by the diffuse reflectance spectra (DRS) (Fig. 3a). Herein, the band gaps of different products were estimated by the following formula [32]:

$$\alpha h\nu = A\,(h\nu - Eg)^2$$

where α is the optical absorption coefficient, $h\nu$ represents photonic energy, A represents proportionality constant, and Eg is the band gap, respectively. One can note that the Pd element could significantly enhance the visible light absorption of Pd/$LaPO_4$, showing a strong harvest over the wavelength range from 520 nm to higher. Also, an increased light harvest from 420 to 480 nm wavelengths could be observed after adding Ag_3PO_4 sensitizer into the Pd/$LaPO_4$. More importantly, after the sunlight illumination, Ag_3PO_4 would be decomposed into Ag nanoparticles so as to give rise the surface plasma resonance of Ag in the nanocomposites, which would dramatically

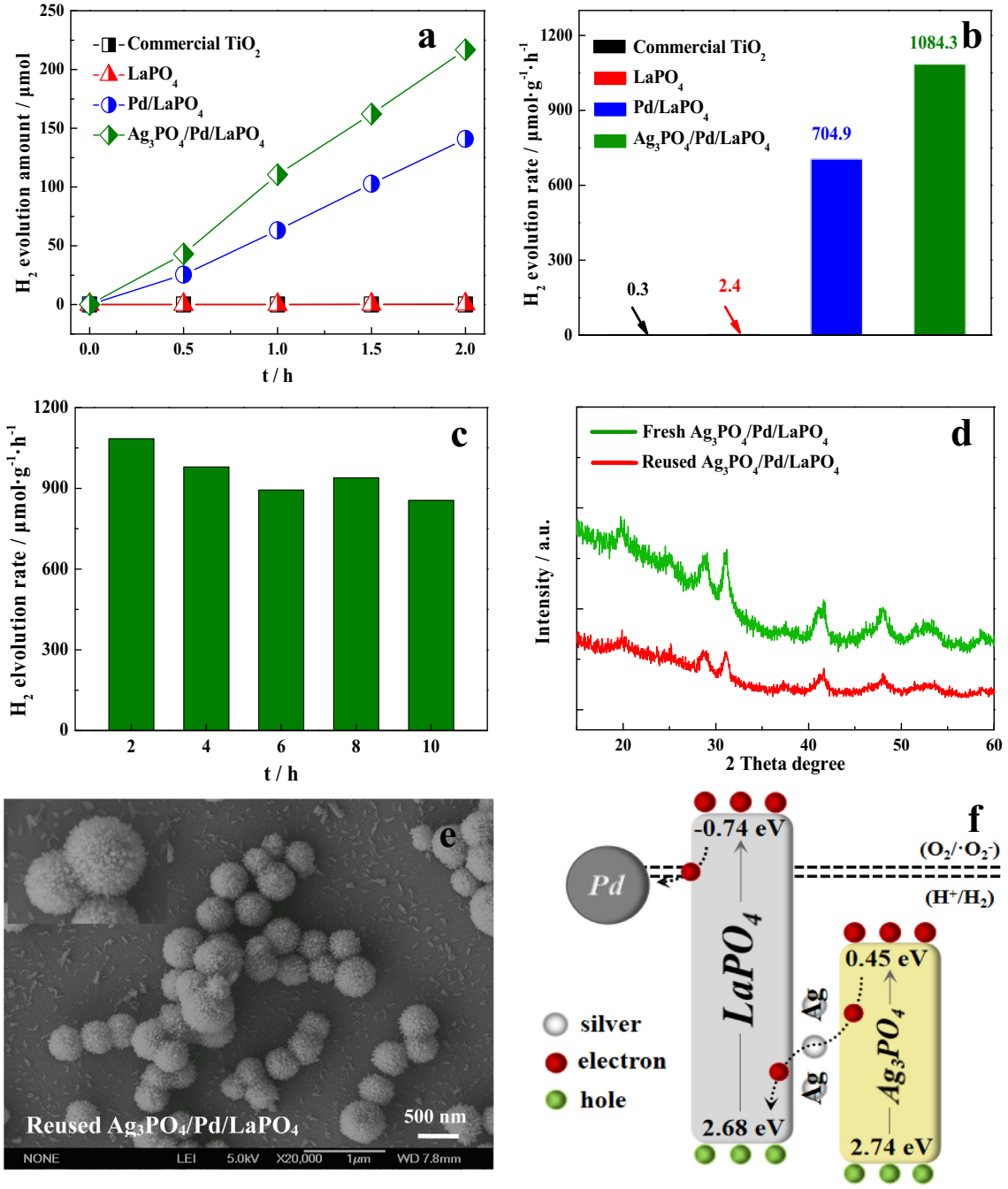

Fig. 4. (a) H_2 production from water using different photocatalysts containing lactic acid as an hole scavenger under simulated sunlight irradiation for 2 h; (b) H_2 evolution rate of different photocatalysts under same conditions; (c) XRD patterns of the Ag_3PO_4/Pd/$LaPO_4$ nanocomposite before and after the photocatalytic reaction; (d) stability test results of Ag_3PO_4/Pd/$LaPO_4$ for five runs in H_2 production; (e) SEM images of reused Ag_3PO_4/Pd/$LaPO_4$ nanocomposite; (f) possible photocatalytic mechanism of Ag_3PO_4/Pd/$LaPO_4$.

enhance the absorption over the range of 360–700 nm. In addition, Fig. 3b manifests that in contrast to Ag_3PO_4 with a band gap energy of 2.29 eV, pure $LaPO_4$ with a band gap energy of 3.42 eV (362 nm of absorption edge) itself may not be efficiently excited by the visible light. Therefore, Pd and Ag_3PO_4 components decorated on $LaPO_4$ can endow the resulting nanocomposites with the enhanced photocatalytic activities, partly due to the broadened solar light harvest.

3.2. Photocatalytic hydrogen evolution and Z-scheme mechanism of Ag_3PO_4/Pd/$LaPO_4$

The photocatalysis performances of Ag_3PO_4/Pd/$LaPO_4$ nanocomposites for the photocatalytic H_2 evolution were comparably assessed, with the data shown in Fig. 4a, b. As revealed in Fig. 4a the synthesized products could have the different abilities in the photocatalytic H_2 generations. Especially, the Ag_3PO_4/Pd/$LaPO_4$ nanocomposites could present the better photocatalytic activity than those of other photocatalysts of TiO_2, $LaPO_4$, and Pd/$LaPO_4$. Moreover, the H_2 evolution rates for commercial TiO_2, $LaPO_4$, Pd/$LaPO_4$ and Ag_3PO_4/Pd/$LaPO_4$ samples were calculated to be 0.30, 2.40, 704.9, and 1084.3 $\mu mol \cdot g^{-1} \cdot h^{-1}$, respectively (Fig. 4b). Apparently, the H_2 evolution rate of Ag_3PO_4/Pd/$LaPO_4$ is over 3600 and 450 times larger than those of commercial TiO_2 and pure $LaPO_4$, respectively. Also, much higher H_2 yield could be obtained for the Ag_3PO_4/Pd/$LaPO_4$

nanocomposites, which could reach 216.9 μmol in the 2 h under simulated sunlight, corresponding to 1084.3 $\mu mol \cdot g^{-1} \cdot h^{-1}$ on average.

The stability tests of photocatalytic hydrogen evolution were carried out by using $Ag_3PO_4/Pd/LaPO_4$. As seen in Fig. 4c, a gradual decrease in the rate of H_2 evolution could be observed for $Ag_3PO_4/Pd/LaPO_4$, which might be attributed to the behavior of photo-decomposition of Ag_3PO_4 materials, slightly challenging the photocatalytic stability of composites. Yet, the favorable photocatalytic stability of nanocomposites could be certified for consecutive uses of five runs. One can note that an increased H_2 evolution rate of $Ag_3PO_4/Pd/LaPO_4$ could be observed at 8 h. Such as phenomenon was thought to be resulted from the fact that during the photocatalytic H_2 evolution reactions, a gradual activation and decomposition of Ag_3PO_4 in $Ag_3PO_4/Pd/LaPO_4$ should occur. As a result, Ag nanoparticles should be released with a suitable quantity at a certain time like 8 h, which would achieve the best separation and transferring efficiencies of photogenerated electron-hole pairs of photocatalysts leading to the irregular enhancement of H_2 evolution. In addition, it was found that the XRD patterns (Fig. 4d) and urchin-like structure (Fig. 4e) of $Ag_3PO_4/Pd/LaPO_4$ could exhibit no obvious variation before and after the photocatalytic reactions, indicating that the nanocomposites could still remain the satisfactory crystal structure and initial morphology.

To investigate the possible photocatalytic mechanism, the energy band structures of $Ag_3PO_4/Pd/LaPO_4$ nanocomposites were investigated with the results shown in Table S2. Accordingly, the valence band potential (E_{VB}) of $LaPO_4$ (2.68 eV) so calculated is more negative than that of Ag_3PO_4 (2.74 eV), which is in consistent with the conduction band potential (E_{CB}) of $LaPO_4$ (−0.74 eV) versus E_{CB} of Ag_3PO_4 (0.45 eV). The data indicate that this well-matched band structures could probably form an expectant heterojunction between $LaPO_4$ and Ag_3PO_4 for effective separation and transfer of photoinduced electrons-hole pairs. On the basis of their energy band potentials and photocatalytic performances, a possible photocatalytic mechanism of $Ag_3PO_4/Pd/LaPO_4$ was thereby proposed in Fig. 4f. The photogenerated electrons from CB of Ag_3PO_4 move to Ag nanoparticles with low work function (4.3 eV) through the Schottky barrier due to the more positive Fermi level and outstanding conductibility of Ag metal [33,34]. Furthermore, the photogenerated electrons from Ag nanoparticles further migrate to the VB of $LaPO_4$ to recombine rapidly with electropositive holes. Subsequently, the detached photogenerated electrons on the CB of $LaPO_4$ are captured by Pd nanoparticles with high work function (5.1 eV) for transforming H_2O (O_2) into H_2 ($\cdot O_2^-$). Therefore, the developed photocatalyst can feature the functions of Ag_3PO_4 (electron donors) and Pd (electron reduction) for the photocatalytic hydrogen evolution and organic pollutants degradation under sunlight. In addition, although the CB potential of Ag_3PO_4 is more positive than that of E_0 (H^+/H_2) and E_0 ($O_2/\cdot O_2^-$) [35], an enhanced H_2 production can still be acquired for the photocatalytic reactions (Fig. 4a), indicating that the photo-induced electrons might migrate from Ag_3PO_4 to $LaPO_4$ rather than from $LaPO_4$ to Ag_3PO_4. According to the description for other nanocomposites (i.e., Ag_3PO_4/In_2S_3 and Ag/AgBr/BiOBr) [29,36,37], the obtained results above inspired us to believe that the developed $Ag_3PO_4/Pd/LaPO_4$ might conduct the *Z*-scheme manner in the photocatalytic reactions. Accordingly, the generated Ag nanoparticles might serve as the bridges to establish the Z-scheme heterojunction at the interface of $LaPO_4$ and Ag_3PO_4, suggesting that the pathways of electron migration might be converted from the conventional “downstairs” to the novel “upstairs”. Hence, this manner can conspicuously enhance the reduction ability of photogenerated electrons toward the improve photocatalytic H_2 evolution.

To further verify the hypothesis above, DMPO electron spin resonance (ESR) tests were performed to validate if the existence of $\cdot O_2^-$ and ·OH in the photocatalytic reactions, aiming to testify the construction of *Z*-scheme manner [38–40]. As shown in Fig. 5a, no peaks were discovered in the darkness. However, four strong characteristic peaks of DMPO-$\cdot O_2^-$ could be perceived in methanol while $Ag_3PO_4/Pd/LaPO_4$ was illuminated by visible light after 10 min. Similarly, typical signal of DMPO-·OH was observed in Fig. 5b, implying the ·OH could also be continually generated during the photocatalytic process. Hence, the results of ESR were in good agreement with the data of the capture experiments, suggesting that the developed nanocomposites could feature the Z-scheme system for the efficient photocatalytic reactions. In addition, the active species capture experiments were performed to further attest the establishment of Z-scheme manner as described elsewhere [20,34,35], with the data shown in Fig. S4. Accordingly, the $\cdot O_2^-$ (rather than ·OH) should serve as the dominant active substances for the photocatalytic reactions with $Ag_3PO_4/Pd/LaPO_4$, even though the CB potential of Ag_3PO_4 is more positive than that of $LaPO_4$, thus confirming the presence of Z-scheme heterojunction.

3.3. Enhanced photogenerated carriers properties of $Ag_3PO_4/Pd/LaPO_4$

In order to further explore the main reasons for the enhanced photocatalytic activities of $Ag_3PO_4/Pd/LaPO_4$ nanocomposites, the separation efficiencies of photo-induced electron-hole pairs were investigated by the photoluminescence (PL) spectra by taking $LaPO_4$ and $Pd/LaPO_4$ for the comparison (Fig. 6a). In principle, a weaker PL intensity of peak should correspond to a lower recombination rate of photo-induced charge carriers, rendering a more favorable photocatalytic activity [41]. Accordingly, the developed photocatalysts were excited by light energy to attain the PL spectra. It was evidently found from Fig. 6a that $Ag_3PO_4/Pd/LaPO_4$ nanocomposites could exhibit the weakest PL intensity than those of other products, indicating that the synergistic effects of $Ag_3PO_4/Pd/LaPO_4$ components could satisfyingly promote the separation efficiency of photo-induced electron-hole pairs toward the high capacity for the photocatalytic H_2 evolution.

Moreover, electrochemical impedance spectroscopy (EIS) measurements were comparably performed to explore the photo-induced charge transfer process (Fig. 6b), in which a smaller semicircle radius should signify a faster charge carriers transfer [42]. One can note from Fig. 6b that the arc radius of $Ag_3PO_4/Pd/LaPO_4$ exhibits the better electrical conductivity and smaller transfer resistance of charge carriers than those of $LaPO_4$ and $Pd/LaPO_4$ products, implying that the photo-generated charge carriers could transfer rapidly through the interface of distinct semiconductors in the photocatalytic system of $Ag_3PO_4/Pd/LaPO_4$. As a result, the transfer velocity of photogenerated charge carriers could be expedited obviously due to the efficient synergistic effects between $LaPO_4$ and $AgPO_4$ materials in the photocatalytic nanocomposites.

4. Conclusion

In summary, urchin-like $LaPO_4$ photocatalyst with integrated Pd and Ag_3PO_4 have been successfully synthesized simply by using a controlled self-assembly route at the assistance of citric acid. Herein, Pd (electron acceptor) and Ag_3PO_4 (electron donor) as different functional components of active sites were introduced on the surface of $LaPO_4$, leading to the improved separation and transfer ability of photogenerated charge carriers for the photocatalytic reactions. Meantime, Ag nanoparticles decomposed from Ag_3PO_4 could serve as the bridges to feature the *Z*-scheme system of nanocomposites, so that the reduction ability of photogenerated electrons could be significantly enhanced. Comparable investigations indicate that the developed photocatalysts could exhibit > 3600 times higher rates of photocatalytic H_2 evolution than the commercial TiO_2. Moreover, urchin-like $LaPO_4$ carries could endow the Pd and Ag_3PO_4 components so anchored with the strong steric hindrance, resulting in the high morphological stability to promise for repeated photocatalytic uses. Importantly, this controlled self-assembly route should not only facilitate the synthesis of urchin-like $LaPO_4$ carries, but also circumvent the enhanced photogenerated carriers properties of different functional components integrated in the nanocomposites, as testified by PL and EIS analysis. It may open a new

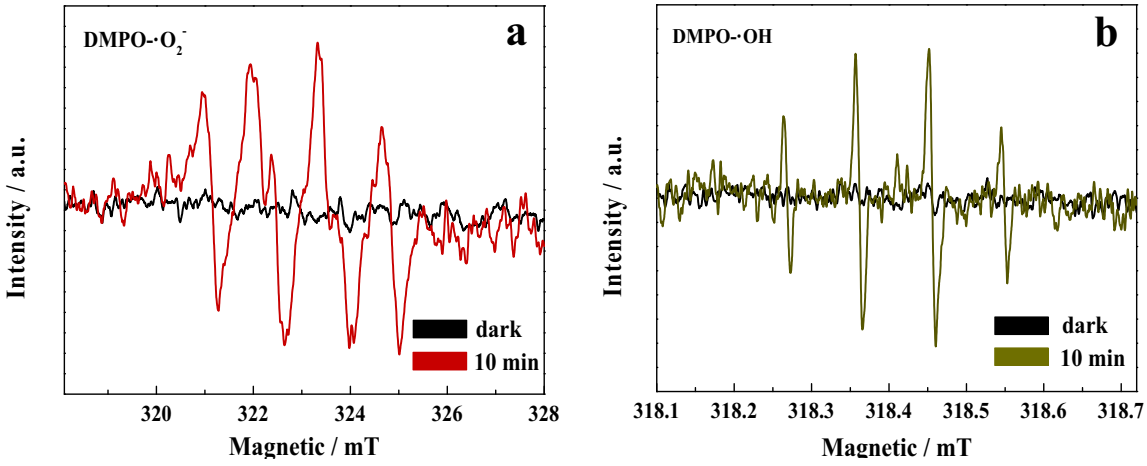

Fig. 5. (a) spin-trapping ESR spectra of $Ag_3PO_4/Pd/LaPO_4$ in methanol for $\cdot O_2^-$ and (b) in water for ·OH.

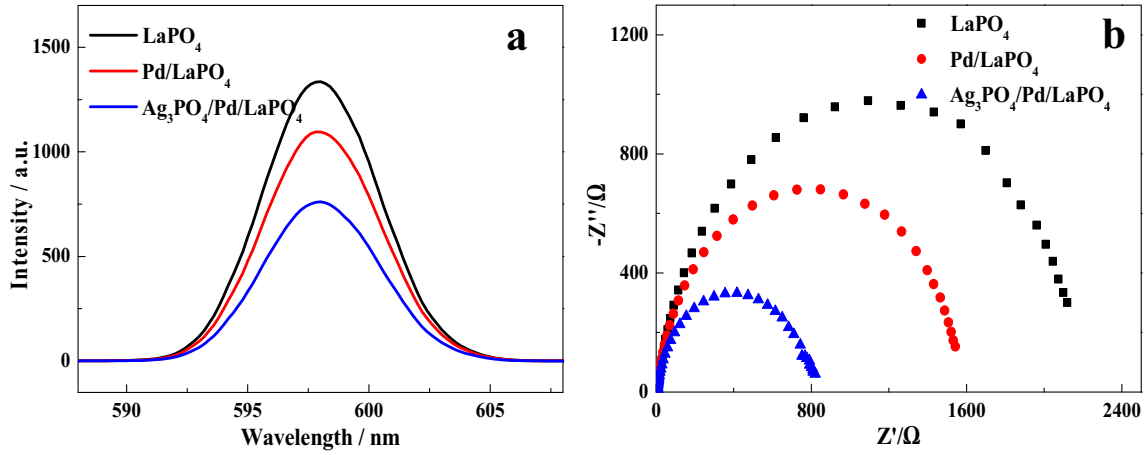

Fig. 6. (a) PL spectra of different products; (b) Nyquist plots for EIS of different products.

door toward the efficient fabrication of multi-component photocatalyst with highly stable structure and especially novel Z-scheme heterojunction to promise for highly H_2 evolution under sunlight.

Acknowledgements

This work was supported by the National Natural Science Foundation of China (No. 21675099); Major Basic Research Program of Natural Science Foundation of Shandong Province, P.R. China (ZR2018ZC0129), and Weihai Science and Technology Development Program (2015DXGJZD002), Shandong Province, P.R. China.

Appendix A. Supplementary data

Supplementary data to this article can be found online at https://doi.org/10.1016/j.apsusc.2019.143771.

References

[1] J. Tian, N. Cheng, Q. Liu, W. Xing, X. Sun, Cobalt phosphide nanowires: efficient nanostructures for fluorescence sensing of biomolecules and photocatalytic evolution of dihydrogen from water under visible light, Angew Chem Int Ed 54 (2015) 5493–5497.
[2] Q. Liu, Z. Pu, A.M. Asiri, A.H. Qusti, A.O. Al-Youbi, X. Sun, One-step solvothermal synthesis of MoS_2/TiO_2 nanocomposites with enhanced photocatalytic H_2 production, J Nanopart Res 15 (2013) 2057.
[3] Z. Zhu, P. Huo, Z. Lu, Y. Yan, Z. Liu, W. Shi, C. Li, H. Dong, Y. Yuan, Y. Yang, Z. Li, D. Chen, S. Wu, G. Fang, W. Bai, M. Ding, L. Yang, D. Cao, Z. Yu, Z. Zou, Promoting charge separation in g-C_3N_4/graphene/MoS_2 photocatalysts by two-dimensional nanojunction for enhanced photocatalytic H_2 production, ACS Appl Energy Mater 1 (2018) 1400–1407.
[4] Z. Jiang, W. Wan, H. Li, S. Yuan, H. Zhao, P.K. Wong, A hierarchical Z-scheme α-Fe_2O_3/g-C_3N_4 hybrid for enhanced photocatalytic CO_2 reduction, Adv Mater 30 (2018) 1706108.
[5] T. Di, Q. Xu, W. Ho, H. Tang, Q. Xiang, J. Yu, Review on metal sulphide-based Z-scheme photocatalysts, ChemCatChem 11 (2019) 1394–1411.
[6] J. Jiang, X. Zhang, P. Sun, L. Zhang, ZnO/BiOI heterostructures: photoinduced charge-transfer property and enhanced visible-light photocatalytic activity, J Phys Chem C 115 (2011) 20555–20564.
[7] S. Adhikari, D.H. Kim, Synthesis of Bi_2S_3/Bi_2WO_6 hierarchical microstructures for enhanced visible light driven photocatalytic degradation and photoelectrochemical sensing of ofloxacin, Chem Eng J 354 (2018) 692–705.
[8] Z. You, Y. Su, Y. Yu, H. Wang, T. Qin, F. Zhang, Q. Shen, H. Yang, Preparation of g-C_3N_4 nanorod/$InVO_4$ hollow sphere composite with enhanced visible-light photocatalytic activities, Appl Catal B Environ 213 (2017) 127–135.
[9] Z. Lu, C. Li, J. Han, L. Wang, S. Wang, L. Ni, Y. Wang, Construction 0D/2D heterojunction by highly dispersed Ni_2P QDs loaded on the ultrathin g-C_3N_4 surface towards superhigh photocatalytic and photoelectric performance, Appl Catal B Environ 237 (2018) 919–926.
[10] Z. Wu, J. Liu, Q. Tian, W. Wu, Efficient visible light formaldehyde oxidation with 2D P-N heterostructure of BiOBr/$BiPO_4$ nanosheets at room temperature, ACS Sustain Chem Eng 5 (2017) 5008–5017.
[11] Y. Zhang, S.J. Park, Au–Pd bimetallic alloy nanoparticle-decorated $BiPO_4$ nanorods for enhanced photocatalytic oxidation of trichloroethylene, J Catal 355 (2017) 1–10.
[12] M. Li, L. Zhang, X. Fan, M. Wu, M. Wang, R. Cheng, L. Zhang, H. Yao, J. Shi, Core-shell $LaPO_4$/g-C_3N_4 nanowires for highly active and selective CO_2 reduction, Appl Catal B Environ 201 (2017) 629–635.
[13] K. Wang, W. Yao, F. Teng, Y. Zhu, Photocatalytic activity enhancement of $LaPO_4$ via surface oxygen vacancy, RSC Adv 5 (2015) 56711–56716.
[14] Z. Yang, G. Huang, W. Huang, Jia. Wei, X. Yan, Y. Liu, C. Jiao, Z. Wan, A. Pan, Novel Ag_3PO_4/CeO_2 composite with high efficiency and stability for photocatalytic applications, J Mater Chem A 2 (2014) 1750–1756.
[15] W. Liu, J. Shen, X. Yang, Q. Liu, H. Tang, Dual Z-scheme g-$C_3N_4/Ag_3PO_4/Ag_2MoO_4$

ternary composite photocatalyst for solar oxygen evolution from water splitting, Appl Surf Sci 456 (2018) 369–378.
[16] M. Hsieh, H. Su, P. Hsieh, Y. Chiang, M.H. Huang, Synthesis of Ag_3PO_4 crystals with tunable shapes for facet dependent optical property, photocatalytic activity, and electrical conductivity examinations, ACS Appl Mater Interfaces 9 (2017) 39086–39093.
[17] R. Qu, W. Zhang, N. Liu, Q. Zhang, Y. Liu, X. Li, Y. Wei, L. Feng, Antioil Ag_3PO_4 nanoparticle/polydopamine/Al_2O_3 sandwich structure for complex wastewater treatment: dynamic catalysis under natural light, ACS Sustain Chem Eng 6 (2018) 8019–8028.
[18] D. Li, H. Wang, H. Tang, X. Yang, Q. Liu, Remarkable enhancement in solar oxygen evolution from $MoSe_2/Ag_3PO_4$ heterojunction photocatalyst via in situ constructing interfacial contact, ACS Sustain Chem Eng 7 (2019) 8466–8474.
[19] X. Cui, L. Tian, X. Xian, H. Tang, X. Yang, Solar photocatalytic water oxidation over Ag_3PO_4/g-C_3N_4 composite materials mediated by metallic Ag and graphene, Appl Surf Sci 430 (2018) 108–115.
[20] X. Chen, W. Zhang, L. Zhang, L. Feng, J. Wen, J. Yang, C. Zhang, J. Jiang, H. Wang, Effective photocatalytic salicylic acid removal under visible light irradiation using Ag_2S/AgI-Bi_2S_3/BiOI with Z-scheme heterojunctions, Appl Surf Sci 481 (2019) 1335–1343.
[21] Q. Xu, L. Zhang, J. Yu, S. Wageh, A.A. Al-Ghamdi, M. Jaroniec, Direct Z-scheme photocatalysts: principles, synthesis, and applications, Mater Today 21 (2018) 1042–1063.
[22] X. Chen, L. Li, W. Zhang, Y. Li, Q. Song, L. Dong, Fabricate globular flower-like CuS/$CdIn_2S_4$/$ZnIn_2S_4$ with high visible light response via microwave-assisted one–step method and its multipath way photoelectron migration properties for hydrogen evolution and pollutant degradation, ACS Sustain Chem Eng 4 (2016) 6680–6688.
[23] Z. Hou, F. Chen, J. Wang, C.P. François-Xavier, T. Wintgens, Novel Pd/$GdCrO_3$ composite for photo-catalytic reduction of nitrate to N_2 with high selectivity and activity, Appl Catal B Environ 232 (2018) 124–134.
[24] Y. Zhu, Z. Xu, W. Jiang, S. Zhong, L. Zhao, S. Bai, Engineering on the edge of Pd nanosheet cocatalysts for enhanced photocatalytic reduction of CO_2 to fuels, J Mater Chem A 5 (2017) 2619–2628.
[25] X. Xie, C. Mao, X. Liu, L. Tan, Z. Cui, X. Yang, S. Zhu, Z. Li, X. Yuan, Y. Zheng, K.W.K. Yeung, P.K. Chu, S. Wu, Tuning the band gap of photo-sensitive polydopamine/Ag_3PO_4/graphene oxide coating for rapid, noninvasive disinfection of implants, ACS Cent Sci 4 (2018) 724–738.
[26] M.N. Shaddad, D. Cardenas-Morcoso, P. Arunachalam, M. García-Tecedor, M.A. Ghanem, J. Bisquert, A. Al-Mayouf, S. Gimenez, Enhancing the optical absorption and interfacial properties of $BiVO_4$ with Ag_3PO_4 nanoparticles for efficient water splitting, J Phys Chem C 122 (2018) 11608–11615.
[27] A. Kar, A. Datta, A. Patra, Fabrication and optical properties of core/shell CdS/$LaPO_4$: Eu nanorods, J Mater Chem 20 (2010) 916–922.
[28] P. Gomathisankar, K. Hachisuka, H. Katsumata, T. Suzuki, K. Funasaka, S. Kaneco, Photocatalytic hydrogen production from aqueous Na_2S + Na_2SO_3 solution with B-doped ZnO, ACS Sustain Chem Eng 1 (2013) 982–988.
[29] X. Chen, R. Li, X. Pan, X. Huang, Z. Yi, Fabrication of In_2O_3-Ag-Ag_3PO_4 composites with Z-scheme configuration for photocatalytic ethylene degradation under visible light irradiation, Chem Eng J 320 (2017) 644–652.
[30] W. Gao, X. Zhang, X. Su, F. Wang, Z. Liu, B. Liu, J. Zhan, H. Liu, Y. Sang, Construction of bimetallic Pd-Ag enhanced AgBr/TiO_2 hierarchical nanostructured photocatalytic hybrid capillary tubes and devices for continuous photocatalytic degradation of VOCs, Chem Eng J 346 (2018) 77–84.
[31] B. Pan, Y. Zhou, W. Su, X. Wang, Self-assembly synthesis of $LaPO_4$ hierarchical hollow spheres with enhanced photocatalytic CO_2 reduction performance, Nano Res 10 (2017) 534–545.
[32] H. Li, Z. Su, S. Hu, Y. Yan, Free-standing and flexible Cu/Cu_2O/CuO heterojunction net: a novel material as cost-effective and easily recycled visible-light photocatalyst, Appl Catal B Environ 207 (2017) 134–142.
[33] Z.M. Yang, G.F. Huang, W.Q. Huang, J.M. Wei, X.G. Yan, Y.Y. Liu, C. Jiao, Z. Wan, A. Pan, Novel Ag_3PO_4/CeO_2 composite with high efficiency and stability for photocatalytic applications, J Mater Chem A 2 (2014) 1750–1756.
[34] L. Ye, J. Liu, C. Gong, L. Tian, T. Peng, L. Zan, Two different roles of metallic Ag on Ag/AgX/BiOX (X = Cl, Br) visible light photocatalysts: surface plasmon resonance and Z-scheme bridge, ACS Catal 2 (2012) 1677–1683.
[35] T. Yan, J. Tian, W. Guan, Z. Qiao, W. Li, J. You, B. Huang, Ultra-low loading of Ag_3PO_4 on hierarchical In_2S_3 microspheres to improve the photocatalytic performance: the cocatalytic effect of ag and Ag_3PO_4, Appl Catal B Environ 202 (2017) 84–94.
[36] Y. He, L. Zhang, B. Teng, M. Fan, New application of Z-scheme Ag_3PO_4/g-C_3N_4 composite in converting CO_2 to fuel, Environ Sci Technol 49 (2015) 649–656.
[37] Z. Chen, W. Wang, Z. Zhang, X. Fang, High-efficiency visible-light-driven Ag_3PO_4/AgI photocatalysts: Z-scheme photocatalytic mechanism for their enhanced photocatalytic activity, J Phys Chem C 117 (2013) 19346–19352.
[38] X. Yang, L. Tian, X. Zhao, H. Tang, Q. Liu, G. Li, Interfacial optimization of g-C_3N_4-based Z-scheme heterojunction toward synergistic enhancement of solar-driven photocatalytic oxygen evolution, Appl Catal B Environ 244 (2019) 240–249.
[39] H. Guo, C. Niu, L. Zhang, X. Wen, C. Liang, X. Zhang, D. Guan, N. Tang, G. Zeng, Construction of direct Z-scheme AgI/$Bi_2Sn_2O_7$ nanojunction system with enhanced photocatalytic activity: accelerated interfacial charge transfer induced efficient Cr (VI) reduction, tetracycline degradation and *Escherichia coli* inactivation, ACS Sustain Chem Eng 6 (2018) 8003–8018.
[40] B. Shao, X. Liu, Z. Liu, G. Zeng, Q. Liang, C. Liang, Y. Cheng, W. Zhang, Y. Liu, S. Gong, A novel double Z-scheme photocatalyst $Ag_3PO_4/Bi_2S_3/Bi_2O_3$ with enhanced visible-light photocatalytic performance for antibiotic degradation, Chem Eng J 368 (2019) 730–745.
[41] S. Shenawi-Khalil, V. Uvarov, S. Fronton, I. Popov, Y. Sasson, A novel heterojunction BiOBr/bismuth oxyhydrate photocatalyst with highly enhanced visible light photocatalytic properties, J Phys Chem C 116 (2012) 11004–11012.
[42] G. Tan, L. She, T. Liu, C. Xu, H. Ren, A. Xia, Ultrasonic chemical synthesis of hybrid mpg-$C_3N_4/BiPO_4$ heterostructured photocatalysts with improved visible light photocatalytic activity, Appl Catal B Environ 207 (2017) 120–133.